Annales Geophysicae, 23, 665–673, 2005
SRef-ID: 1432-0576/ag/2005-23-665

Annales Geophysicae

A statistical study of gravity waves from radiosonde observations at Wuhan (30° N, 114° E) China

S. D. Zhang[1,2] **and F. Yi**[1,2]

[1]Department of Electronic Engineering, Wuhan University, Wuhan, People's Republic of China
[2]Key Laboratory of Geospace Environment and Geodesy, Ministry of Education, Wuhan, People's Republic of China

Received: 21 April 2004 – Revised: 27 January 2005 – Accepted: 29 January 2005 – Published: 30 March 2005

Abstract. Several works concerning the dynamical and thermal structures and inertial gravity wave activities in the troposphere and lower stratosphere (TLS) from the radiosonde observation have been reported before, but these works were concentrated on either equatorial or polar regions. In this paper, background atmosphere and gravity wave activities in the TLS over Wuhan (30° N, 114° E) (a medium latitudinal region) were statistically studied by using the data from radiosonde observations on a twice daily basis at 08:00 and 20:00 LT in the period between 2000 and 2002. The monthly-averaged temperature and horizontal winds exhibit the essential dynamic and thermal structures of the background atmosphere. For avoiding the extreme values of background winds and temperature in the height range of 11–18 km, we studied gravity waves, respectively, in two separate height regions, one is from ground surface to 10 km (lower part), and the other is within 18–25 km (upper part). In total, 791 and 1165 quasi-monochromatic inertial gravity waves were extracted from our data set for the lower and upper parts, respectively. The gravity wave parameters (intrinsic frequencies, amplitudes, wavelengths, intrinsic phase velocities and wave energies) are calculated and statistically studied. The statistical results revealed that in the lower part, there were 49.4% of gravity waves propagating upward, and the percentage was 76.4% in the upper part. Moreover, the average wave amplitudes and energies are less than those at the lower latitudinal regions, which indicates that the gravity wave parameters have a latitudinal dependence. The correlated temporal evolution of the monthly-averaged wave energies in the lower and upper parts and a subsequent quantitative analysis strongly suggested that at the observation site, dynamical instability (strong wind shear) induced by the tropospheric jet is the main excitation source of inertial gravity waves in the TLS.

Keywords. Meteorology and atmospheric dynamics (Waves and tides; Climatology; General or miscellanous)

Correspondence to: S. D. Zhang
(zsd@whu.edu.cn)

1 Introduction

Gravity waves and their associated momentum transportation and energy propagation are believed to have a significant impact on local tropospheric and lower stratospheric climatology (Alexander and Pfister, 1995; Alexander, 1998). It is well known that in the middle and upper atmosphere, gravity waves play an important role in determining the global dynamic and thermal structures (Lindzen, 1981; Holton, 1982, 1983; Garcia and Solomon, 1985), and are responsible for local short-term variability of background atmosphere and large-scale atmospheric waves (Fritts and Vincent, 1987). Gravity waves in the middle and upper atmosphere are believed to be excited mainly in the troposphere and lower stratosphere (TLS) and propagate upward (Alexander, 1996), resulting in energy coupling between the lower and upper atmosphere. Therefore, it is of significant importance to study the basic features of gravity wave activities in the TLS.

Radiosonde observations were initially used for studying local meteorology. In each measurement of radiosonde, accompanying the free ascent of a balloon, meteorological variables, such as pressure, temperature and relative humidity, are measured. The horizontal winds can be attained by tracking the position of the balloon, which allows us to determine the horizontal propagation directions of gravity waves. The typical height coverage of the radiosonde observation is from ground surface up to 25–30 km, the uncertainty of the upper limit height is due to the uncertain burst height of the balloon. Recently, radiosondes were extensively applied to study the dynamics and gravity waves in the TLS for its excellent height resolution (several tens of meters to several hundreds of meters) (Tsuda et al., 1994a,b; Shimizu and Tsuda, 1997; Pfenninger et al., 1999; Vincent and Alexander, 2000; Yoshiki and Sato, 2000; Zink and Vincent, 2001a,b). Many radiosonde observations suggested that the dominant gravity wave disturbances in the TLS were inertial gravity waves, usually having a vertical wavelength of several kilometers, horizontal wavelength of several hundreds of kilometers, and a horizontal wind disturbance amplitudes of several ms^{-1}.

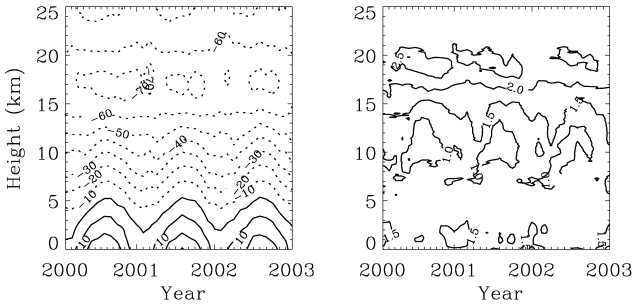

Fig. 1. Time-height cross sections of monthly-averaged temperature in °C (left) and buoyancy frequency in 10^{-2} rad s^{-1}(right). The dotted contours denote the negative values.

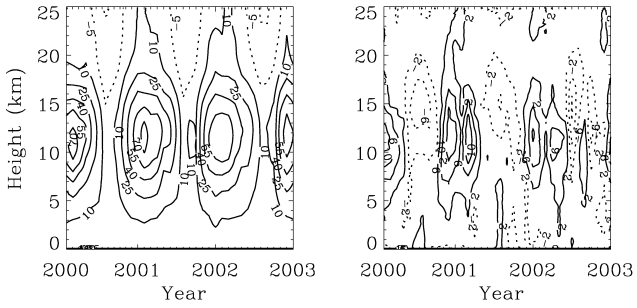

Fig. 2. Time-height cross sections of monthly-averaged zonal (left) and meridional (right) winds. Dotted contours denote the negative (westward and southward) values.

The data utilized in early studies of radiosonde observations were based on specific campaigns (Tsuda et al., 1994a,b; Shimizu and Tsuda, 1997), which had limited time coverage. The most recent studies have begun to use the radiosonde data acquired routinely by meteorological agencies (Pfenninger et al., 1999; Vincent and Alexander, 2000; Yoshiki and Sato, 2000; Zink and Vincent, 2001a,b). Observations at different latitudinal regions have revealed that the dynamics and gravity wave activities in the TLS have an obvious latitudinal variation (Allen and Vincent, 1995; Vincent and Alexander, 2000; Yoshiki and Sato, 2000; Zink and Vincent, 2001a,b). Based on observations, many modeling works were developed to parameterize the impacts of gravity waves on the climatology of the TLS (Alexander and Vincent, 2000; Vincent et al., 1997). However, they are far away from comprehensively understanding the global dynamics of the TLS, which pushes us to study the gravity wave activities in the TLS in a broader latitudinal range. The radiosonde observations cited above are concentrated either in low-latitudinal (or equatorial) (Tsuda et al., 1994a,b; Shimizu and Tsuda, 1997) or high-latitudinal (or polar) regions (Pfenninger et al., 1999; Vincent and Alexander, 2000; Yoshiki and Sato, 2000; Zink and Vincent, 2001a,b); most observations in the mid-latitudinal region are from VHF radar (Fritts et al., 1990; Murayama, 1994; Sato, 1994), which cannot provide us with the density and temperature profiles. The radiosonde observational results in the medium latitudinal area were sparsely reported.

The main purpose of this paper is to statistically study the gravity wave characteristics in the mid-latitudinal TLS. The data utilized in this paper is from the radiosonde observation at Wuhan (30° N, 114° E) in the period between 2000 and 2002; a detailed description of data and background observation is presented in Sect. 2. A similar data processing method to that proposed by Vincent and Alexander (2000) is adopted in this paper, which is introduced in Sect. 3. The statistical results of the observed gravity waves are given in Sect. 4 In Sect. 5, we discuss the possible sources of gravity waves in the TLS, and the primary conclusions are drawn in the last section.

2 Data description and background observation

Radiosonde observations made by the Wuhan Center Station of Meteorology on a twice daily basis at 08:00 and 20:00 LT in the period between 2000 and 2002 were used in this study. The raw data are sampled at 8-s intervals, resulting in an uneven height resolution, which varies from 10 m to 100 m. For convenience, the raw data were processed to have an even height resolution (100 m) by applying a linear interpolation. The maximum altitude of radiosonde observation is the burst height of the balloon. In our data set, about 52% of measurements reached a height of 25 km, but only about 18% reached 27 km. Thus, we chose 25 km as the upper height limit of our analysis.

Figure 1 shows the monthly-averaged temperature and buoyancy frequency within the period from 2000 to 2002 in the height range from the ground surface to 25 km. The temperatures show obvious fluctuation with time below the height about 14 km, which is different with the radiosonde observation in the equatorial regions (Vincent and Alexander, 2000). Above 14 km, they vary little over the 3 years of observation. The tropopause height roughly estimated from Fig. 1 is at a height of about 14 km. An extremely low temperature less than $-70°$ C around a height of 17 km can be observed. The coldest temperature above the tropopause occurs in June, and annual cycles can be observed, but they are not as regular as they were at the tropical region (Reid and Gage, 1996; Vincent and Alexander, 2000). Below the height of 15 km, the buoyancy frequency show slow variability with time and height, the value varies from 0.01 to 0.015 rad s^{-1}; above the height of 18 km, it is almost a constant value 0.025 rad s^{-1}.

Figure 2 is the monthly-averaged zonal and meridional winds. Below the height of 3 km, the zonal wind fields are very weak. Within the height range 3–15 km, the zonal winds are eastward and usually increase with height up to about 11.5 km, with maximum values about 70 ms^{-1} and then decrease with height, which indicates a strong tropospheric jet around 11.5 km. Moreover, an evident annual cycle can also be observed. Above the height of 18 km up to 25 km, different from the observation of the lower latitudinal region (Vincent and Alexander, 2000), the zonal wind field

is dominated by the annual oscillation rather than the quasi-biennial oscillation, with a mean flow of ~ -5 to $10\,\mathrm{ms}^{-1}$; a rough division shows that the westward wind field occurs in the period from June to November, and an eastward wind in the other half of the year. Compared with the zonal wind, the meridional wind is rather weaker and usually less than $10\,\mathrm{ms}^{-1}$. In the height range 5–20 km, the meridional wind fields are southward in winter and northward in summer. The strongest southward wind often occurs at a height near 15 km in July, with a maximum value of $-6\,\mathrm{ms}^{-1}$. Differently, the strongest northward wind occurs at a lower height near 11.5 km, with a larger maximum value of $10\,\mathrm{ms}^{-1}$; moreover, the maximum value occurs twice a year in March and December, respectively.

3 Extraction of quasi-monochromatic gravity waves

For obtaining the parameters for quasi-monochromatic gravity waves, we should correctly remove the background winds and temperature from the raw data. The usual data processing method takes the temporal averaged values as the background state; however this is not feasible for the radiosonde observation due to its large temporal intervals. Here we calculated the background $[u_0, v_0, T_0]$ by fitting a second-order polynomial to the vertical profiles of horizontal winds and temperature $[u, v, T]$, respectively; in order to avoide the extreme values of temperature near the heights of about 17.5 km (shown in Fig. 1) and those of the horizontal winds in the heights range between 11–15 km (shown in Fig. 2); the fittings are taken individually to two separate height ranges: one is the lower part, which is from the ground surface to 10 km; the other (upper part) is from 18 to 25 km. Then the fluctuation components $[u_f, v_f, T_f]$ can be derived from the raw data $[u, v, T]$ by removing the background. The quasi-monochromatic wave components $[u', v', T']$ are extracted by a harmonic fitting to the fluctuation components as the following equation:

$$U = A\sin(\frac{2\pi}{\lambda_z}z + \varphi), \tag{1}$$

where, U=$[u_f, v_f, T_f]$ is the fluctuation component, A=$[A_u, A_v, A_T]$ and φ=$[\varphi_u, \varphi_v, \varphi_T]$ are the fitted amplitude and phase of the quasi-monochromatic components, respectively; λ_z is the vertical wavelength, which varies at a 100-m step length from 200 m to 10 and 7 km for the lower and upper parts, respectively. Obviously, in the harmonic fitting, different $\lambda_z$will result in different amplitudes; we take the value of λ_z with the maximum fitted amplitude as the dominant vertical wavelength. Considering that the dominant wavelengths for different wave components (e.g. zonal wind, meridional wind and temperature) may be different, the average value of these three dominant wavelengths is taken to be the wavelength of the derived quasi-monochromatic gravity wave. Only when the relative standard error of three dominant wavelengths is less than 20%, do we think that a quasi-monochromatic gravity wave is observed. Having specified the vertical wavelength, we re-take the harmonic fitting to determine the wave's amplitudes and phases for each wave components.

Figure 3 gives the typical example of a quasi-monochromatic gravity wave in the lower part observed on 18 February 2002. Figure 3d is the profile of wave disturbance temperatures T' normalized by the background temperature $T_0(z)$, and the percentage temperature fluctuation of 1% is observed. The vertical wavelength is calculated to be 6.6 km. The zonal and meridional amplitudes are about 6.5 and $4.0\,\mathrm{ms}^{-1}$, respectively. The hodograph of horizontal disturbances is an ellipse, and the asterisk and plus symbols demonstrate that the disturbance wind vector rotates anti-clockwise. According to the polarization relation for inertial gravity waves, the anti-clockwise rotating hodograph indicates that in the Northern Hemisphere, the gravity wave energy is propagating downward. Figure 4 is similar to Fig. 3, but for a gravity wave in the upper part. For the gravity wave shown in Fig. 4, the vertical wavelength is 4.2 km, and the zonal and meridional disturbance amplitudes are about $1.0\,\mathrm{ms}^{-1}$, which are smaller than those in the lower part. It is noticeable that the hodograph of horizontal disturbance indicates that the gravity wave energy is propagating upward, different from that in the lower part, which suggests that there is a force source for gravity waves within the intermediate part (10 and 18 km) between the lower and upper parts.

4 Statistical results

4.1 Wave intrinsic frequencies

By analyzing the polarization relation for inertial gravity waves, we know that the horizontal propagation direction of a gravity wave is along the major axial of its horizontal wind vector hodograph, and the horizontal perturbation velocities parallel (u_{para}) and perpendicular (u_{perp}) to the major axial of the horizontal wind vector hodograph satisfy the following equation:

$$\frac{u_{perp}}{u_{para}} = -i\frac{f}{\Omega} \tag{2}$$

where Ω and f($7.29\times10^{-5}\,\mathrm{rads}^{-1}$ at Wuhan) denote the wave intrinsic frequency and local Coriolis frequency, respectively. Equation (2) implies that the ratio of Ω to f is equal to that of the major to minor axes of the hodographs shown in Figs. 3 and 4 (Tsuda et al., 1990; Eckermann, 1996), then the wave intrinsic frequency can be easily calculated. For example, the intrinsic frequencies of the gravity waves shown in Figs. 3 and 4 are calculated to be 2.6 and 2.5 times of the Coriolis frequency, respectively. However, too large a ratio of Ω to f will cause many uncertainties (Vincent and Alexander, 2000; Zink and Vincent, 2001); thus, a cut-off value of 10 is chosen in this paper. Then, 791 and 1165 quasi-monochromatic gravity waves were extracted from our three-years data set for the lower and upper parts, respectively.

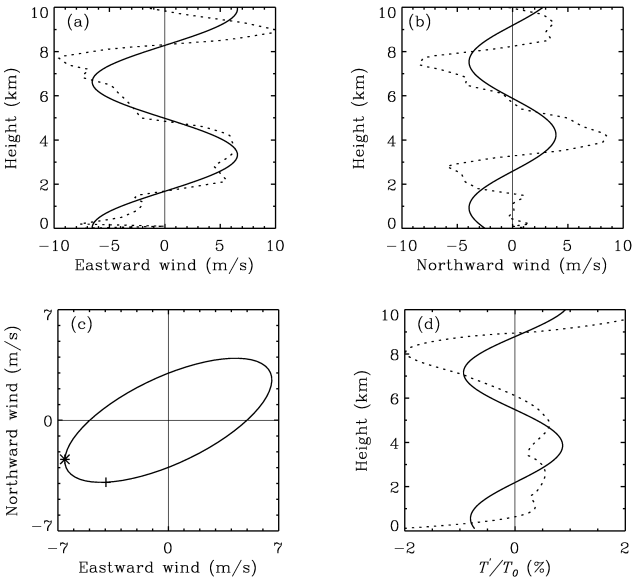

Fig. 3. Vertical profiles of zonal (**a**) and meridional (**b**) disturbance components of the derived quasi-monochromatic gravity wave, and percentage normalized temperature fluctuations (**d**) observed on 18 February 2002 at 08:00 LT. The solid and dotted lines denote the wave disturbance and fluctuation components, respectively. (**c**) is the hodograph of the horizontal wind wave disturbance components, where the asterisk and plus symbols denote the values at the height of 0 and 1 km, respectively.

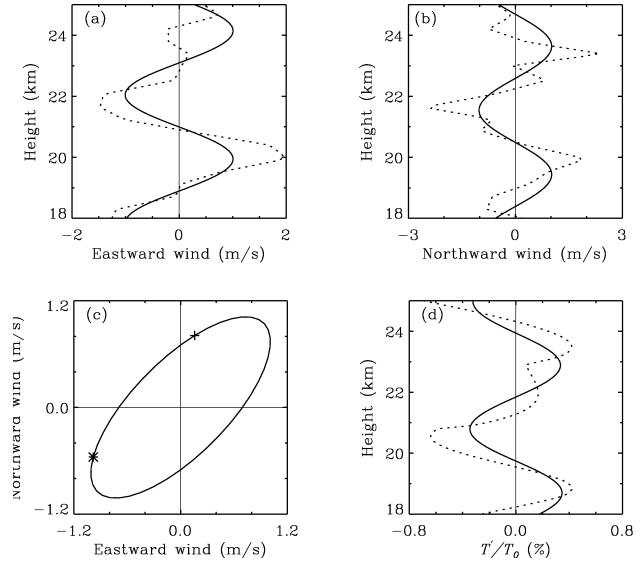

Fig. 4. Vertical profiles of zonal (**a**) and meridional (**b**) disturbance components of the derived monochromatic gravity wave, and percentage normalized temperature fluctuations (**d**) observed on 18 February 2002, at 08:00 LT. The solid and dotted lines denote the wave disturbance and fluctuation components, respectively. (**c**) is the hodograph of the horizontal wind wave disturbance components, where the asterisk and plus symbols denote the values at the height of 18 and 19 km, respectively.

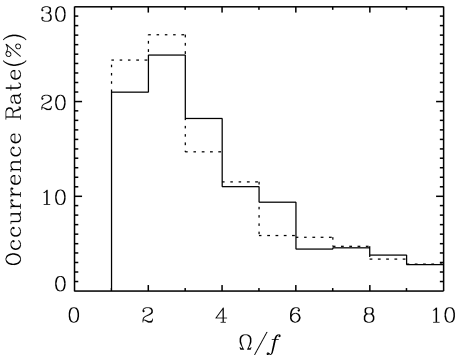

Fig. 5. Histogram of $\frac{\Omega}{f}$. The solid and dotted lines denote the occurrence rates of gravity waves in the lower and upper parts, respectively.

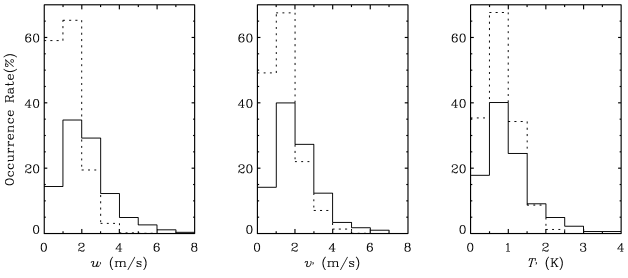

Fig. 6. Histograms of gravity wave amplitudes. The left and middle panels are the zonal and meridional wind disturbance amplitudes u' and v', respectively; and the temperature disturbance amplitude T' is shown in the right panel. The solid and dotted lines denote the occurrence rates of gravity waves in the lower and upper parts, respectively.

Figure 5 is the histogram of the intrinsic frequencies normalized to the Coriolis frequency. In Fig. 5, it is observed that most gravity waves have a frequency that is less than 4 times that of the Coriolis frequency and with peak occurrence rates of 25% and 27% in the frequency range 2–3 times that of Coriolis frequency in the lower and upper parts, respectively, indicating that the dominant gravity wave disturbance in the TLS over Wuhan is an inertial gravity wave. This is consistent with the observations at other sites.

4.2 Wave amplitudes

Figure 6 gives the distribution of wave amplitudes. For the gravity waves in both the lower and upper parts, their horizontal wind amplitudes are smaller than $8\,\mathrm{ms}^{-1}$, and their temperature amplitudes are no larger than 4 K. These wave amplitudes are much smaller than those attained in the equatorial region (Vincent and Alexander, 2000), suggesting that the gravity wave amplitudes are latitudinal dependence. Zhang and Yi (2004) have numerically studied the latitudinal dependency of gravity wave amplitudes, and attributed it to a kind of nonlinear effect. Another possible reason may be the latitudinal dependence of wave sources. In the lower part, most gravity waves have horizontal wind

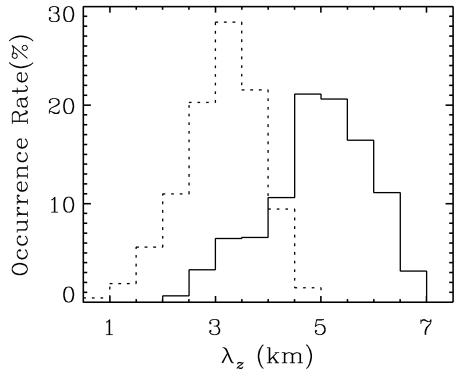

Fig. 7. The same as in Fig. 5, but for vertical wavelengths.

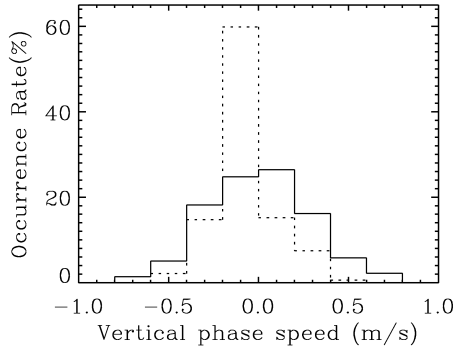

Fig. 8. The same as in Fig. 5, but for vertical intrinsic phase velocities.

amplitudes of 1–3 ms^{-1} and temperature amplitudes of 0.5–1.5 K. Compared with the gravity waves in the lower part, those in the upper part have smaller wave amplitudes, concentrating in 1–2 ms^{-1} and 0.5–1 K for the horizontal wind and temperature amplitudes, respectively.

4.3 Vertical wavelengths and propagation directions

The distribution of vertical wavelengths was calculated and shown in Fig. 7. The vertical wavelengths for gravity waves in the lower part varied from 2–7 km and with a dominant scale range 4.5–5.5 km. Gravity waves in the upper part have a rather different vertical wavelength distribution, with a dominant wavelength range of 2.5–4 km. The vertical intrinsic phase speed can be easily attained from the expression of $\frac{\Omega}{\lambda_z}$, and the direction (upward or downward) can be derived from the hodograph of the wind vector, as introduced in Sect. 3.

Figure 8 gives the histogram of vertical intrinsic phase speeds. For gravity waves in the lower part, their vertical intrinsic phase velocities are concentrated around zero and with a rather symmetric distribution around zero, 49.4% of the waves have negative phase speeds (upward wave energy propagation). An obviously different result was observed in the upper part. In the range of -0.2–$0\,ms^{-1}$, the occurrence rate of vertical intrinsic phase speeds has a prominent peak value of 60%, and 76.7% of the waves are propagating

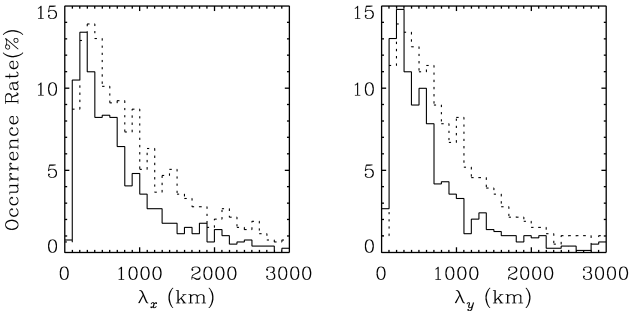

Fig. 9. The same as in Fig. 5, but for the zonal (left panel) and meridional (right panel) wavelengths.

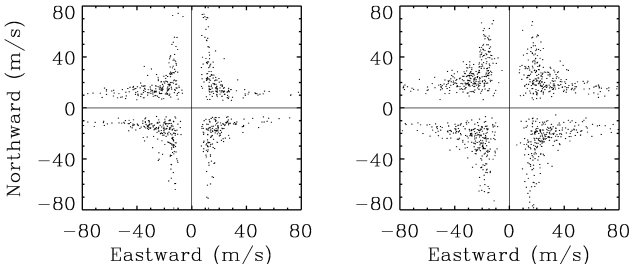

Fig. 10. Distributions of the intrinsic horizontal phase speeds for gravity waves in the lower (left panel) and upper parts (right panel).

upward; this percentage is close to the observation (72%) by Vincent and Alexander (2000), indicating that the main force sources for the gravity waves in the lower stratosphere are below the height of 18 km.

4.4 Horizontal wavelengths and propagation directions

As mentioned in Subsect. 4.1, the horizontal propagation direction of a gravity wave is along the major axial of its horizontal wind vector hodograph; then the horizontal wave number can be deduced from the simplified dispersion equation for inertial gravity waves

$$k_{zonal}^2 + k_{meridional}^2 = \frac{k_{vertical}^2(\Omega^2 - f^2)}{N^2}, \quad (3)$$

where k_{zonal}, $k_{meridional}$ and $k_{vertical}$ are the zonal, meridional and vertical wave numbers, respectively. The signs of horizontal wave numbers can be derived from the polarization of gravity waves. For example, the zonal and meridional wave numbers for the case shown in Fig. 3 are derived to be -1.19×10^{-5}(eastward positive) and 0.70×10^{-5} rad m^{-1} (northward positive), respectively, and those values for the gravity wave shown in Fig. 4 are, respectively, $0.35\times10^{-5}$and -0.99×10^{-5} rad m^{-1}. A histogram of the horizontal wavelengths is displayed in Fig. 9, while the distribution of intrinsic horizontal phase velocities is shown in Fig. 10. For the observed gravity waves, their horizontal wavelengths vary from several tens of km to 3000 km, which are much larger than their vertical wavelengths, suggesting that they are propagating at very shallow angles to

Table 1. Mean values of gravity wave parameters. The "Lower" and "Upper" mean the gravity waves in the lower and upper parts, respectively, and the over bars denote a unweighted average over the whole observation period.

	$\overline{\frac{\Omega}{f}}$	$\overline{u'}$ (ms^{-1})	$\overline{v'}$ (ms^{-1})	$\overline{T'}$ (K)	$\overline{\lambda_z}$ (km)	$\overline{\lambda_x}$ (km)	$\overline{\lambda_y}$ (km)	$\overline{E}$ ($J\,kg^{-1}$)
Lower	4.2	2.2	2.1	1.0	5.4	744	665	14
Upper	4.1	1.3	1.4	0.8	3.6	940	864	2

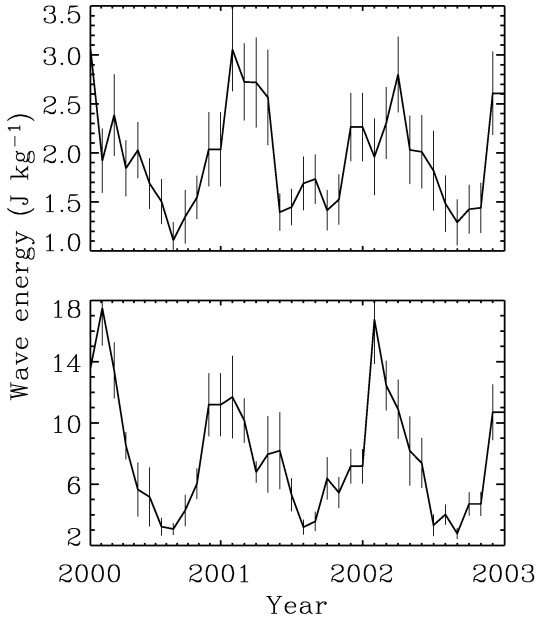

Fig. 11. Time series of monthly-averaged wave energies per unit mass in the lower (bottom panel) and upper parts (top panel). The vertical bars give the standard errors for the averaged values.

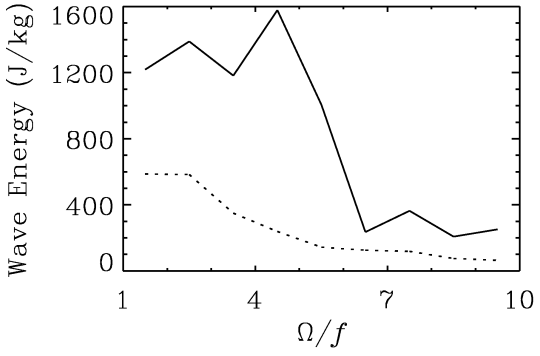

Fig. 12. Frequency distributions of wave energies for inertial gravity waves in the lower (solid curve) and upper parts (dotted curve).

the horizontal. Figure 10 illustrates that the observed gravity waves have a horizontal intrinsic phase speed usually larger than $10\,ms^{-1}$. The dominant horizontal propagation direction of gravity waves in the lower part is westward, against the background wind, however, for gravity waves in the upper part, their horizontal propagations are rather symmetric and no obvious dominant directions are observed.

4.5 Wave energies

Wave energy per unit mass is computed from

$$E = \frac{1}{2}(\overline{u'^2} + \overline{v'^2} + \overline{w'^2} + \overline{\frac{g^2 T'^2}{N^2 T_0^2}}), \quad (4)$$

where the over bar denotes an unweighted average over height. We have no measurements of vertical winds, but in fact compared with horizontal wind, it is much smaller and will not contribute significantly to wave energy, thus, in our computation, $\overline{w'^2}$ is omitted. Figure 11 gives the time variability of monthly-averaged gravity wave energies. Obvious seasonal variations can be seen from Fig. 11, and for the gravity waves in both the lower and upper parts have a similar time variability, except that the wave energy in the upper part is much smaller. Intensive gravity wave activities occur in winter and spring, and weaker gravity wave activity usually occurs in summer, which is also similar to the seasonal variation of the background zonal wind.

4.6 Mean wave parameters

Table 1 summaries the mean wave parameters. A comparison between the mean parameters of gravity waves in the lower and upper parts shows that the disturbance amplitudes and wave energies of gravity waves in the lower part are larger than those in the upper part; as to the spatial scales, the gravity waves in the lower part have larger vertical wavelengths; and shorter horizontal wavelengths, these discrepancies may due to different time and height variability of the background atmosphere in the two parts.

5 Discussion

Restricted by the height coverage of radiosonde observations and the nature of the adopted hodograph analysis method, we can only study the properties of gravity waves with lower frequencies and vertical wavelengths of several kilometers, which was discussed by Alexander (1996). In order to address the influences of the hodograph analysis method on the results, we calculated the frequency distributions of wave energies for gravity waves in the lower and upper parts, respectively. Seeing from Fig. 12, both in the lower and upper parts,

most wave energies were carried by a low-frequency (smaller than 5 times and 3 times that of the Coriolis frequency in the lower and upper parts, respectively) gravity wave. Compared with the low-frequency components, the wave energies carried by the gravity waves with higher frequencies are negligible, indicating that the influences of the adopted hodograph analysis method are not significant, as anticipated.

An apparently similar time variability of the monthly-averaged wave energies for the gravity waves in the lower and upper parts was shown in Fig. 11. The correlative coefficient between them was calculated to be 0.62, which suggested that gravity waves in the lower and upper parts may have the same main generation sources. Focusing on the possible generation sources of gravity waves in the TLS, we calculated, respectively, the correlative coefficients between the background kinetic energy and gravity waves in the lower and upper parts and plotted them in Fig. 13. These two profiles of correlative coefficients are rather close to each other: The correlative coefficients are very small in the height ranges below 3 km and above 20 km, indicating that the topography in these regions has little impact on the actions of the observed gravity waves. However, the radiosonde observations in the polar regions (Yoshiki and Sato, 2000) revealed that topography is an important gravity wave source, indicating that the gravity wave sources have a latitudinal dependence in TLS region, which leads to the latitudinal dependence of gravity waves properties (wave amplitudes and energies). Within the height range from 5 to 17 km, the correlative coefficients are very large and with maxima values larger than 0.8, so large correlative coefficients have never been reported before.

The evidently correlated time evolutions of wave energies in the lower and upper parts suggests two possible wave sources: A first possibility is that the wave source is within the lower part, which means that the upward propagating gravity waves observed in the upper part may be excited originally in the lower part. It should be noted that there are 890 (corresponding to a 76.4% percentage) gravity waves propagating upward in the upper part, but only 391 (corresponding to a 49.4% percentage) gravity waves propagate upward in the lower part. Moreover, when a gravity wave, especially for the low-frequency gravity wave, propagates upward from the lower part through the tropospheric jet to the upper part, it may encounter its critical layer and be captured by the background, which means that the intermediate atmosphere between the lower and upper parts will intensively absorb the wave energy and halt the gravity waves in the lower part before reaching the heights of the upper part. Therefore, a conclusion can be drawn that although part of the gravity waves in the upper part may be excited in the lower part, the main wave source is out of the lower part.

Another possibility is that there are intensive wave sources in the intermediate atmosphere between the lower and upper parts (10–18 km). Considering the background wind structure shown in Fig. 2, a possible wave source is the tropospheric jet which occurs around the height of 11.5 km. Usually, the tropospheric jet means strong wind shear, which

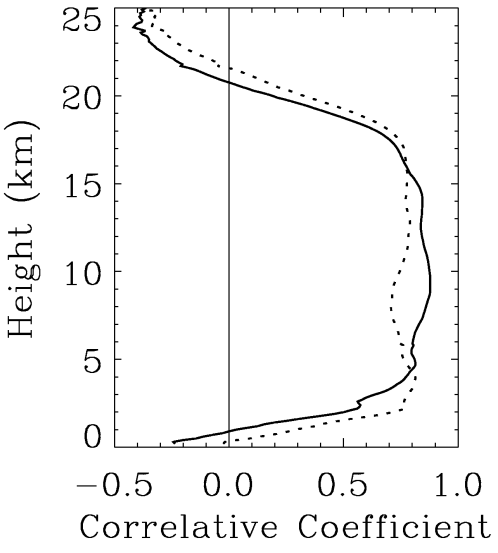

Fig. 13. Profiles of correlative coefficients of monthly-averaged background kinetic energy with monthly-averaged energies for gravity waves in the lower (solid line) and upper (dotted line) parts.

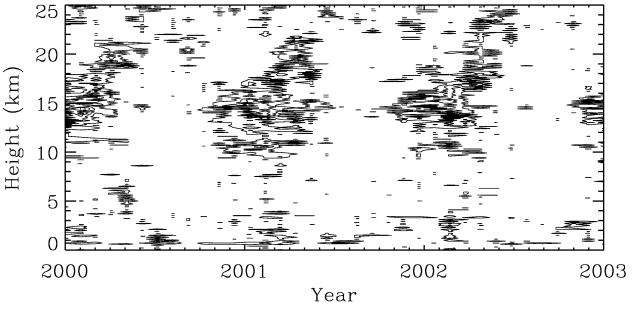

Fig. 14. Contours of the occurrence rate of dynamic instability. The minimum and interval of the contours are 3%.

leads to dynamic instability. Therefore, we calculated the Richardson number, Ri , for the background atmosphere, where $Ri=\frac{N^2}{\left(\frac{\partial \bar{u}}{\partial z}\right)^2+\left(\frac{\partial \bar{v}}{\partial z}\right)^2}$. When $Ri<\frac{1}{4}$, then the dynamical instability occurs. For the sake of discriminating the dynamical instability induced by convection instability ($N^2<0$ or $Ri<0$), hereinafter, we define the term "dynamical instability" to mean that the Richardson number satisfies $0<Ri<\frac{1}{4}$. Figure 14 illustrates the occurrence rate of the dynamical instability for each month; which is defined by $\frac{N_{di}}{N_m}$, for each month, N_{di} denotes the number of occurrences of a dynamical instability within a month and N_m denotes the total number of measurements in a month. It is observed from Fig. 14 that the temporal variation of the occurrence rate in the intermediate part is rather similar to that of the wave energy shown in Fig. 12. For further studying the relationship between the wave energy and the dynamical instability, we calculated the correlative coefficients of the occurrence rate of dynamical instability with monthly-averaged gravity wave energies (plotted in Fig. 15). In Fig. 15, large correlative

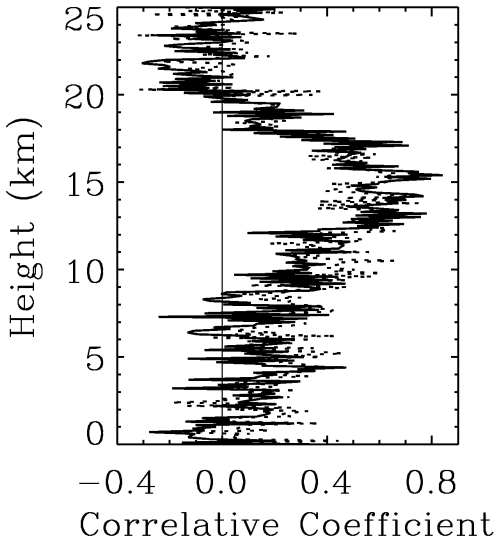

Fig. 15. Profiles of correlative coefficients of the occurrence rate of dynamical instability with monthly-averaged energies for gravity waves in the lower (solid line) and upper (dotted line) parts.

coefficients (larger than 0.8) can be seen in the intermediate part. Moreover, a similar analysis was carried out for studying the relationship between the convection instability and the gravity wave activities, but no obvious correlativity can be found. All above the discussions strongly suggest that the strong wind shear owning to the tropospheric jet is the main excitation source for the gravity waves both in the lower and upper parts.

6 Conclusions

Data from radiosonde observations made by the Wuhan Center Station of Meteorology on a twice daily basis at 08:00 and 20:00 LT in the period between 2000 and 2002 were used to statistically study the background atmosphere and gravity wave activities in the TLS.

The monthly-averaged temperature shows an obvious fluctuation with time below the height about 14 km, and above this height, they vary little over the 3 years of observation. The tropopause is estimated at a height of about 14 km. Above the tropopause, an extremely low temperature of less than $-70°$ C at a height of about 17 km is observed. As to the monthly-average zonal mean wind fields, above the height of 18 km up to 25 km, it is dominated by the quasi-annual oscillation. Compared with the zonal wind, the meridional wind is weaker.

There were 791 and 1165 quasi-monochromatic gravity waves extracted from our three-year data set in the lower (from 0 to 10 km) and upper (from 18 to 25 km) parts, respectively. A statistical analysis shows the main characteristics of the gravity waves in the TLS over Wuhan: inertial frequency gravity waves are the dominant gravity wave disturbances; vertical and horizontal wavelengths are of several kilometers and several hundreds of kilometers, respectively; the horizontal winds and temperature disturbance amplitudes are of several $\mathrm{m\,s^{-1}}$ and K, respectively; the horizontal intrinsic phase speeds are of several tens of $\mathrm{ms^{-1}}$.

Compared with the gravity waves in the lower part, those in the upper part have smaller amplitudes and vertical wavelengths, but larger horizontal wavelengths. The dominant horizontal propagation direction of gravity waves in the lower part is westward, which is against the background wind, however, for gravity waves in the upper part; their horizontal propagations are rather symmetric and no dominant directions are observed. In the lower part, 49.4% of gravity waves are propagating upward, and the percentage is 76.7% in the upper part.

The monthly-averaged gravity wave energies in the lower and upper parts show obvious seasonal variation and are rather similar, indicating that the main excitation sources for the gravity waves in the two parts may be the same. The correlative coefficients between the background kinetic energy and gravity wave energies have prominent peak values (larger than 0.8) within the intermediate part between the lower and upper parts. More detailed analysis strongly suggests that, different from the polar area, the dynamical instability induced from the tropospheric jet is the main excitation source of gravity waves in the TLS over Wuhan.

Acknowledgements. We wish to thank the anonymous reviewer for his valuable suggestions on this paper. This work was jointly supported by the National Natural Science Foundation of China (through grant 40336054 and 40274051) and the Program for New Century Excellent Talents in University of China.

Topical Editor U.-P. Hoppe thanks a referee for his help in evaluating this paper.

References

Alexander, M. J.: A simulated spectrum of convectively generated gravity waves: Propagation from the tropopause to the mesopause and effects on the middle atmosphere, J. Geophys. Res., 101, 1571–1588, 1996.

Alexander, M. J.: Interpretations of observed climatological patterns stratospheric gravity wave variance, J. Geophys. Res., 103, 8627–8640, 1998.

Alexander, M. J. and Pfister, L.: Gravity wave momentum flux in the lower stratosphere over convection, Geophys. Res. Lett., 22, 2029–2032, 1995.

Alexander, M. J. and Vincent, R. A.: Gravity waves in the tropical lower stratosphere: A model study of seasonal and interannual variability, J. Geophys. Res., 105, 17 983–17 993, 2000.

Allen, S. J. and Vincent, R. A.: Gravity-wave activity in the lower atmosphere: Seasonal and latitudinal variations, J. Geophys. Res., 100, 327–1350, 1995.

Eckermann, S. D.: Hodograph analysis of gravity waves: Relationships among Stokes parameters, rotary spectra and cross-spectral methods, J. Geophys, Res., 101, 19 169–19 174, 1996.

Fritts, D. C. and Vincent, R. A.: 1987: Mesospheric momentum flux studies at Adelaide, Australia: observations and a gravity wave-tidal interaction model, J. Atmos. Sci., 44, 605–619, 1987.

Fritts, D. C., Tsuda, T., VanZandt, T. E., Smith, S. A., Sato, T., Fukao, S., and Kato, S.: Studies of velocity fluctuations in the lower atmosphere using the MU radar, II, Momentum fluxes and energy densities, J. Atmos. Sci., 47, 51–66, 1990.

Garcia, R. R. and Solomon, S.: The effects of breaking gravity waves on the dynamics and chemical composition of the mesosphere and lower thermosphere, J. Geophys. Res., 90, 3850–3868, 1985.

Holton, J. R.: The role of gravity wave-induced drag and diffusion in the momentum budget of the mesosphere, J. Atmos. Sci., 39, 791–799, 1982.

Holton, J. R.: The influence of gravity wave breaking on the general circulation of the middle atmosphere, J. Atmos. Sci., 40, 2497–2507, 1983.

Lindzen, R. S.: Turbulence and stress owing to gravity wave and tidal breakdown, J. Geophys. Res., 86, 9707–9714, 1981.

Murayama, Y., Tsuda, T., and Fukao, S.: Seasonal variation of gravity wave activity in the lower atmosphere observed with the MU radar, J. Geophys., Res., 99, 23 057–23 069, 1994.

Pfenninger, M. A., Liu, A. Z., Papen, G. C. and Gardner, C. S.: Gravity wave characteristics in the lower atmosphere at South Pole, J. Geophys. Res., 104, 5963–5984, 1999.

Reid, G. C. and Gage, K. S.: The tropical tropopause over the western Pacific: Wave driving, convection and the annual cycle, J. Geophys. Res., 101, 21 233–21 241, 1996.

Sato, K.: A statistical study of the structure, saturation and sources of inertio-gravity waves in the lower stratosphere observed with the MU radar, J. Atmos. Sol. Terr. Phys., 56, 755–774, 1994.

Shimizu, A. and Tsuda, T.: Characteristics of Kelvin waves and gravity waves observed with radiosondes over Indonesia, J. Geophys. Res., 102, 26 159–26 171, 1997.

Tsuda, T., Kato, S., Yokoi, T., Inoue, T., and Yamamoto, M.: Gravity waves in the mesosphere observed with the middle and upper atmosphere radar, Radio Sci., 25, 1005–1018, 1990.

Tsuda, T., Murayama, Y., Wiryosumarto, H., Harijono, S. W. B., and Sato, S.: Radiosonde observations of equatorial atmosphere dynamics over Indonesia, 1, Equatorial waves and diurnal tides, J. Geophys. Res., 99, 10 491–10 506, 1994a.

Tsuda, T., Murayama, Y., Wiryosumarto, H., Harijono, S. W. B., and Sato, S.: Radiosonde observations of equatorial atmosphere dynamics over Indonesia, 2, Characteristics of gravity waves, J. Geophys. Res., 99, 10 491–10 506, 1994b.

Vincent, R. A. and Alexander, M. J.: Gravity waves in the tropical lower stratosphere: An observational study of seasonal and interannual variability, J. Geophys. Res., 105, 17 971–17 982, 2000.

Vincent, R. A., Allen, S. J., and Eckermann, S. D.: Gravity wave parameters in the lower stratosphere, in Gravity Wave Processes: Their Parameterization in Global Climate models, K. Hamilton (Ed.), NATO ASI Ser. I, 50, 7–25, 1997.

Yoshiki, M. and Sato, K.: A statistical study of gravity waves in the polar regions based on operational radiosonde data, J. Geophys. Res., 105, 17 995–18 011, 2000.

Zhang, S. D. and Yi, F.: A numerical study on global propagations and amplitude growths of large scale gravity wave packets, J. Geophys. Res., 109, D07106, doi:10.1029/2003JD004429, 2004.

Zink, F. and Vincent, R. A.: Wavelet analysis of stratospheric gravity wave packets over Macquarie Island, 1. Wave parameters, J. Geophys. Res., 106, 10 275–10 288, 2001a.

Zink, F. and Vincent, R. A.: Wavelet analysis of stratospheric gravity wave packets over Macquarie Island, 2. Intermittency and mean-flow accelerations, J. Geophys. Res., 106, 10 289–10 297, 2001b.